# Stress Effects in Cylindrical Tubes of Austenitic and Ferritic/Martensitic Steels with Oxide Scales

## - Materials Selection for a HPLWR -

H. Steiner

Institut für Materialforschung

Programm Nukleare Sicherheitsforschung

**Abstract**

In the frame of the studies for a high performance concept of a Light Water Reactor (LWR) different materials for the cladding are investigated, among them are austenitic and ferritic/martensitic (f/m) steels of different Cr content. Due to the envisaged very extended life times of the fuel elements in the reactor, corrosion problems may arise. Thus, cracking and/or spalling effects in oxide scales on metallic components may play an important role in the corrosion process as they lead, in general, to a drastic enhancement in the oxidation rates.

Analytical models for different fundamental stress problems in the compound oxide scale/ metallic substrate have been developed and implemented in the computer code OXSPA. These models concern the growth stresses in the cylindrical tubes, the stresses due to temperature changes and radial temperature gradients and the stresses due to inside and outside pressures.

# Spannungseffekte durch Oxidschichten auf zylindrischen Rohren aus austenitischen und ferritisch/martensitischen Stählen

**Zusammenfassung**

Im Rahmen der Studien für ein Hochleistungskonzept eines Leichtwasserreaktors (LWR) werden verschiedene Hüllmaterialien auf ihre Eignung hin untersucht, unter anderem auch austenitische und ferritisch/martensitische Stähle. Aufgrund der vorgesehenen sehr langen Standzeiten der Brennelemente im Reaktor können Korrosionsprobleme auftreten. Dabei können Rissbildungen und Abplatzvorgänge in den Oxidschichten zu einer drastischen Erhöhung der Oxidationsraten führen.

Dazu wurden analytische Modelle zur Beschreibung von verschiedenen fundamentalen Spannungsproblemen im Verbund aus Oxidschicht und metallischem Substrat entwickelt und in den Computercode OXSPA eingebaut. Diese Modelle betreffen im einzelnen die Wachstumsspannungen in zylindrischen Rohren, die mechanischen Spannungen durch Temperaturwechsel und durch radiale Temperaturgradienten in den Hüllrohren und die Spannungen durch innere und äußere Drücke.

**CONTENTS** <u>Page</u>

Notation

Indices

Figures 2 - 14

# 1   Introduction

In the frame of the studies for a high performance concept of a Light Water Reactor (LWR) different materials for the cladding are investigated, among them are austenitic and fer-ritic/martensitic (f/m) steels of different Cr content. Due to the envisaged very extended life times of the fuel elements in the reactor, corrosion problems may arise. Thus, cracking and or spalling effects in oxide scales on metallic components may play an important role in the corrosion process as they lead ,in general, to a drastic enhancement in the oxidation rates.

The modeling of the stress/strain evolutions in the oxide scales and the metallic substrates is an indispensable prerequisite for the understanding of the stress effects. In order to achieve this different numerical methods like finite elements or finite difference solutions of the stress-strain equations do exist. But these methods demand a rather high numerical effort and do not always allow to evidence and understand the influence of the basic physical parameters in an easy manner.

The use of simple analytical models has therefore some advantages in this respect and with such models different stress effects can be investigated rather easily. In this report we have considered growth stresses, stresses due to temperature changes and radial temperature gradients, as well as stresses due inside and outside gas pressures.

# 2   Material data

In this section we have compiled the material data used for the calculations. Of course, the results of the models are very much influenced by the choice of these data and some discussion is worthwhile.

Data for the oxides $Cr_2O_3$ and FeO, $Fe_2O_3$ and $Fe_3O_4$ are rather scarce, especially for the temperature range 600 - 650°C. A review on mechanical properties of oxides is given by M. Schütze /1/. Some data for oxides could also be found in a paper of H.E. Evans /2/ and in the handbook of Gmelin /3/.

The data used for the ferritic and austenitic alloys are mainly from a report of C. Petersen /4/. Concerning the mechanical data it is surprising, that the difference in the Young's modulus of the metallic alloy and that of the respective oxide is so low, especially for the ferritic marten-sitic alloys. It should be noted that the Young's modulus of the oxide is of considerable impor-tance for the stress calculations.

As concerns the Poisson number, the same value has been taken for the oxides and the metallic phase in order to simplify the stress equations a bit. Otherwise ratios of $(1 - \upsilon^{ox})/(1 - \upsilon^{me})$ would appear for the bi-axial stress state. But in any case, these ratios would have values not so far from one.

**Table 1:** Material data used for the stress calculations

| | |
|---|---|
| $\alpha^{me}$  [1/K] | $1{,}8 \cdot 10^{-5}$ (austenite) |
| | $1{,}25 \cdot 10^{-5}$ (ferrite) |
| $\alpha^{ox}$  [1/K] | $0{,}85 \cdot 10^{-5}$ |
| $E^{me}$  [MPa] | $1{,}5 \cdot 10^{5}$ (austenite) |
| | $1{,}7 \cdot 10^{5}$ (ferrite) |
| $E^{ox}$  [MPa] | $2{,}6 \cdot 10^{5}$ (austenite) |
| | $2{,}1 \cdot 10^{5}$ (ferrite) |
| $\nu$  [-] | $0{,}3$ |
| $K_I$  [M/M$^{3/2}$] | $1{,}7$ |
| $\gamma$  [J/m$^2$] | $6$ |

Data for creep and oxidation of some ferritic/martensitic and austenitic alloys have been transmitted by L. Heikinheimo /5/ and M. Schirra /6/. The correlations of the metal loss thickness $\delta^{ox}$ were given in the following form:

$$\delta^{ox}(t) = A \cdot e^{B/T} \cdot t^{1/2} + sp \cdot t \tag{1}$$

The values of the parameters A , B, and sp are to be found in table 2.

**Table 2:**  Parameter values for the metal loss correlation for different selected alloys

| Alloy | Cr content (%) | A ($\mu m/h^{\frac{1}{2}}$) | B (K) | sp (T=650 °C) ($\mu m/h$) |
|---|---|---|---|---|
| ST22 | 2.25 | $1.9004 \ 10^{6}$ | -14402 | $8 \cdot 10^{-3}$ |
| TP91 | 9 | $9.278 \ 10^{3}$ | - 8114 | $6 \cdot 10^{-3}$ |
| HCM12A | 11 | $7.9179 \ 10^{4}$ | -10824 | $<4 \cdot 10^{-4}$ |
| 1.4910 | 16 | $8.368 \ 10^{4}$ | -10897 | $<2 \cdot 10^{-4}$ |
| TP347HFG | | $6.3588 \ 10^{4}$ | -11309 | $<2 \cdot 10^{-4}$ |

Based on these data correlations for the oxide scale thickness $\delta^{ox}$ values for the metal loss thickness $\delta^{me}$ were obtained using:

$$\delta^{me} = 1/2 \cdot \delta^{ox} \tag{2}$$

as the Pilling-Bedworth ratios have values of about 2.

For the creep rate of the metallic substrate $\dot{\varepsilon}$ , the following correlations valid for temperatures around 650 $^0$C have been established based on the data transmitted in /6/:

2

ST22  2.2 wt% Cr

$$\dot{\varepsilon}(\sigma, T) = 2.1 \cdot 10^2 \cdot \sigma^5 \cdot \exp(-55430 / T)$$

TP91  9 wt% Cr

$$\dot{\varepsilon}(\sigma, T) = 1.785 \cdot \sigma^{5.5} \cdot \exp(-80680 / T)$$

NF616  10 wt% Cr

$$\dot{\varepsilon}(\sigma, T) = 2.153 \cdot 10^{10} \, \sigma^{7.5} \, \exp(-72020 / T)$$

HCM12A  11-12 wt% Cr

$$\dot{\varepsilon}(\sigma, T) = 6.7 \cdot 10^9 \, \sigma^{4.8} \, \exp(-55430 / T)$$

1.4910

$$\dot{\varepsilon}(\sigma, T) = 0.958 \cdot 10^{-21} \sigma^{16} \, \exp(-56870 / T)$$

*$\dot{\varepsilon}$ in 1/s      $\sigma$  in Mpa     T in K*


## 3    Model development and discussion of stress effects


In this section simple analytical models for different stress effects due to the presence of oxide scales are developed and discussed. These concern the stresses due to the growth of the oxide scale, the stress effects of temperature changes and that of radial temperature gradients, and the stresses due to inside and outside (gas) pressures.

All these effects are discussed separately in order to establish clearly their respective importance. But according to the circumstances, some of these effects may act concomitantly, and as creep effects in the metallic substrate may play a role, the real situation can be rather complicated.

All the models presented and discussed in the following sections are implemented in the recently developed code OXSPA, which runs on a personal computer. The different models can be selected with the help of a steering parameter.


### 3.1   Growth stresses


Growth stresses arise due to the volume increase caused by the oxygen uptake. The stress state depends on the details of the growth process, that means whether the oxide scale grows on its  outside or on its inside whether growth is isotropic or goes only in radial direction /7/.

In austenitic steels it's predominantly the $Cr^{3+}$ ions which are migrating /8/, therefore the oxide scale is growing at the outside. In ferritic/martensitic alloys the oxide scale consists of several sublayers /9/. As there is oxygen diffusion besides that of $Fe^{2+/3*}$ and $Cr^{3+}$ ions we have inside and outside growth in the oxide scale. Thus, the situation is rather complicated for f/m alloys.

The main assumption is that the growth of the oxide scale goes only in radial direction and that for austenitic as well as for ferritc alloys. On a flat plate there would be in this case no growth stresses, but on a curved surface, as for a cylindrical tube, growth stresses arise. Thus, we have a purely geometrical effect.

By the growth of the scale a point P, which was originally located at the radius a is displaced by the amount u (see fig. 1):
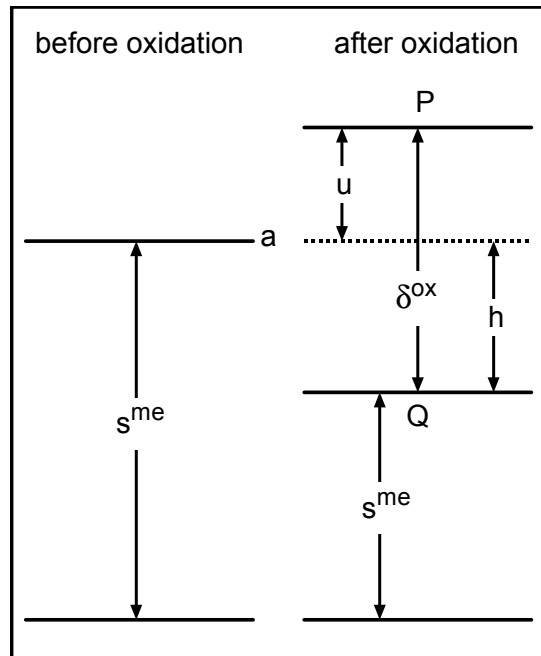


Fig. 1:     Schematic view of the geometrical changes due to oxide scale formation

$$u = \delta^{ox} - h \tag{3}$$

h = thickness of consumed metal layer

The hoop strain at this location is then given as:

$$\varepsilon_\theta^{ox} = \frac{u}{a} \tag{4}$$

and with:

$$\delta^{ox} = h\varphi \tag{5}$$

$\varphi = $ Pilling-Bedworth ratio

we obtain for the hoop strain at the outside of the scale:

$$\varepsilon_\theta^{ox} = \frac{\varphi - 1}{\varphi} \frac{\delta^{ox}}{a} \tag{6}$$

For a flat plate the radius of curvature a would go to infinity and the hoop strain would be zero. With φ = 1 this would also be the case.

4

The point Q at the inside of the scale is undisplaced and has therefore no hoop strain. Between Q and P the hoop strain increases linearly with the radial position.

Due to our assumption that the volume increase goes entirely into the radial direction, there is no axial strain in the scale and the metallic substrate. Therefore we have a mono-axial stress state in the cladding, namely a tensile hoop stress in the scale and a compressive hoop stress in the metallic substrate. Therefore the metallic substrate experiences a contraction $\varepsilon_\theta^{me}$:

$$\varepsilon_\theta^{me} = \frac{\sigma_\theta^{me}}{E^{me}} \tag{7}$$

$\sigma_\Theta{}^{me}$ = mean hoop stress in the metallic substrate

If this is taken into account, we obtain for the median hoop strain in the oxide scale:

$$\overline{\varepsilon_\theta^{ox}} = 1/2 \frac{\varphi - 1}{\varphi} \frac{\delta^{ox}}{a} + \varepsilon_\theta^{me} \tag{8}$$

The mean hoop stresses in the oxide scale $\overline{\sigma_\theta^{ox}}$ and in the metallic substrate are then calculated with the help of:

$$\overline{\sigma_\theta^{ox}} = \overline{\varepsilon_\theta^{ox}} / E^{ox} \tag{9}$$

$$\overline{\sigma_\theta^{ox}} \delta^{ox} + \sigma_\theta^{me} s^{me} = 0 \tag{10}$$

$E^{me}, E^{ox}$ = Young's module of metal and oxide phase

$s^{me}$ = thickness of the metallic substrate

we obtain:

$$\overline{\sigma_\theta^{ox}} = 1/2 \frac{\varphi - 1}{\varphi} \frac{\delta^{ox}}{a} \frac{E^{ox}}{1 + \frac{E^{ox}}{E^{me}} \frac{\delta^{ox}}{s^{me}}} \tag{11}$$

and:

$$\sigma_\theta^{me} = -\overline{\sigma_\theta^{ox}} \frac{\delta^{ox}}{s^{me}} \tag{12}$$

If there is creep in the metallic substrate, due to the mono-axial stress state the equivalent stress and creep strain increment are given as:

$$\sigma_{eq}^{me} = \sigma_\theta^{me} \tag{13}$$

$$\Delta \varepsilon_{eq}^{me} = \Delta \varepsilon_\theta^{me,cr} \tag{14}$$

and the creep increment in the time step $\Delta t$ is then calculated with the help of the creep correlation:

5

$$\Delta\varepsilon_\theta^{me,cr} = \Delta t \cdot \dot{\varepsilon}(\sigma_\theta^{me}, T) \tag{15}$$

In this case, no closed form solution of $\overline{\sigma_\theta^{ox}}$ can be given but this quantity can then be determined with the help of an iterative procedure starting at t = 0 and taking into account the accumulated creep deformation of the metallic substrate in the contraction $\varepsilon_\theta^{me}$ :

$$\varepsilon_\theta^{me} = \frac{\sigma_\theta^{me}}{E^{me}} + \sum_{\Delta t} \Delta\varepsilon_\theta^{me,cr} \tag{16}$$

The iterative procedure is done with the help of the equations (8), (15) and (16). In the oxide scale itself we do not consider creep effects, as the maximum design temperature (650 0C) is distinctly below $0.4 T_m^{ox}$. It should also be noted that the hoop stresses at the inside and the outside of the scale are given as:

$$\sigma_\theta^{ox,i} = E^{ox}\varepsilon_\theta^{me} \tag{17}$$

$$\sigma_\theta^{ox,o} = E^{ox}\left(\frac{\varphi-1}{\varphi}\frac{\delta^{ox}}{a} + \varepsilon_\theta^{me}\right) \tag{18}$$

The foregoing derivation of stresses and strains is based on the assumption that the volume increase due to oxidation is perfectly anisotropic and goes into the radial direction. With this assumption we hope to approximate the real case rather well, but there may, of course, be some isotropic component in the volume change. If one takes this isotropic component into account the hoop stress in the oxide scale is a superposition of an anisotropic and an isotropic component:

$$\sigma_\theta^{ox} = \sigma_\theta^{ox,an} + \sigma_\theta^{ox,iso} \tag{19}$$

with these components given as:

$$\sigma_\theta^{ox,an} = 1/2 \frac{\delta^{ox}}{a}\frac{\overset{\succ}{\varphi}-1}{\overset{\succ}{\varphi}}\frac{E^{ox}}{1+\dfrac{\delta^{ox}}{s^{me}}\dfrac{E^{ox}}{E^{me}}} \tag{20}$$

$$\sigma_\theta^{ox,iso} = -\frac{E^{ox}}{1-v}\frac{\Delta\varepsilon_{sw}^{iso}}{1.+\dfrac{\delta^{ox}}{s^{me}}\dfrac{E^{ox}}{E^{me}}} \tag{21}$$

$$\sigma_z^{ox,iso} = \sigma_\theta^{ox,iso} \tag{22}$$

with:

6

$$\overset{\succ}{\varphi} = \varphi - 3\Delta\varepsilon_{sw}^{iso} \qquad (23)$$

$$\varphi = 1 + 3\Delta\varepsilon_{sw}^{iso} + \Delta\varepsilon_{sw}^{an} \qquad (24)$$

If the volume change is completely isotropic, $\Delta\varepsilon^{an}$ would be zero and equation (21) provides the well-known expression of the hoop stress in this case. It should be noted that the isotropic volume change gives a compressive hoop stress not depending on the radial location. The isotropic component of the stress should have a beneficial effect on the mechanical stability of the oxide scale. Up to a certain value of the thickness the oxide scale remains entirely in a compressive stress state due to the superposition of the isotropic and the anisotropic components of the hoop stress. It would be very interesting to check whether for certain alloys we could obtain a marked effect.

The isotropic contribution could be determined by bending experiments with a flat plate making use of the formula of Stoney/10/:

$$\sigma_{\theta}^{ox,iso} = \frac{E^{ox} s^{me} s^{me}}{6R\delta^{ox}} \qquad (25)$$

R = radius of curvature

For the time being no such bending tests have been done. Therefore, no data on the isotropic component are available. Thus, for the time being we have to stick to our basic assumption of a perfectly anisotropic volume increase going entirely into the radial direction.
Calculations have been done with OXSPA for the f/m alloys ST22, TP91, and HCM12A with 2, 9, and 11 wt% Cr and for the austenitic alloy 1.4910, as oxidation and creep correlations were avaible for these alloys. Only the parabolic contribution of the oxidation correlations have been used in the correlations. Some of the results are to be found in figs. 2 to 7. The growth stresses are most important in the high temperature region of the cladding, as the cladding corrosion increases exponentially with the temperature. Therefore the temperature range between 500 and 650 $^0$C has been investigated. Calculations have been done with and without taking into account the creep of the metallic substrate. The results shown in figs. 2 to 7 were all obtained for a temperature of 600 °C.
In case of no creep effect taken into account, the mean and outside hoop stresses in the scale show a parabolic increase, whereas the elastic contraction of the metallic substrate leads to continuous decrease of the inner hoop stress of the oxide scale. In the inner part of the scale and in the metallic substrate the hoop stresses are compressive, whereas the outer part of the scale is in a tensile stress state. The higher the oxidation rate, the higher and faster rise the tensile hoop stresses. As soon as creep in the metallic substrate comes into play the outside and the mean hoop stress in the oxide scale no longer rise parabolically, but the mean hoop stress even reaches a maximum and then decreases gradually thereafter.

Tensile stresses lead to cracking in the scale when the maximum hoop stress is above the fracture stress. We can learn from our calculations of growth stresses that in the inner part of the scale there should be no cracking and the alloys with high oxidation rates should show more cracking than that with low oxidation rates.
We would expect that for the alloys ST22 and TP91 cracking starts rather early, whereas for HCM12A it is very much later and less severe. It should be noted that the austenitic alloy 1.4910 has practically the same oxidation rates as the f/m alloy HCM12A and therefore also about the same stress evolution.
The fracture stress in the oxide scale is determined by the flaw size c. With $K_I$ being the fracture toughness, we have the following equation for the fracture stress $J_f$:

$$K_I = f \cdot \sqrt{\Pi \cdot c} \cdot \sigma_f \tag{26}$$

For a penny-shaped flaw the geometrical factor f is exactly 1, for other flaw geometries f is a bit different from 1. Thus, this parameter has not a decisive influence.

For a fracture toughness values of 1,7 MN/m$^{3/2}$, we have calculated the fracture stress for the flaw radius c varying between 1 and 100 μm. The results are to be found in table 3. Thus the fracture stress varies between about 100 and 900 MPa.

The flaw size should somewhat be correlated to the thickness of the scale. It is, for example, not possible to have a flaw size of 100 μm in a scale of about 10 μm. If there is a growth of voids and/or pores in the oxide scale due to migration of vacancies, then the flaw size is a function of time and therefore the fracture stress should decrease in the course of the oxidation process.

**Table 3:** Fracture stress values in iron oxides for penny-shaped flaws of different size (K$_I$ = 1,7 MN/m$^{3/2}$)

| Radius of penny-shaped flaw [μm] | Fracture Stress [MPa] |
|---|---|
| 1 | 920 |
| 10 | 290 |
| 100 | 90 |

In /1/ values for tensile fracture strains for $Cr_2O_3$ scales grown on alloy 800H and for bulk chromia are given. The values range from about 0.1% to about 0.4%. For temperatures between 600 and 650 $^0$C the values are between 0.2 and 0.4%. With a value of 2.6e5 Mpa for Young's modulus we obtain fracture stress values between 520 and 1040 Mpa.

In /11/ the following correlation for the oxide failure strain in dependence on the oxide scale thickness is provided:

$$\varepsilon_{frac}^{ox} = (\frac{\gamma_c}{2pE^{ox}\delta^{ox}})^{1/2} \tag{27}$$

with p representing the fraction of the effective flaw size to the oxide scale thickness and $\gamma_c$ being the cohesive fracture energy.

As suggested in /11/ the values p = 0.25 and $\gamma_c/E^{ox}$=4.10$^{-11}$ were used to determine the oxide fracture stress in dependence on the oxide scale thickness. The fracture stress given by this empirical model is shown in fig. 8. For very small oxide scales we obtain fracture stress values of more than 2000 Mpa. For oxide scales above 100 μm the fracture stress falls below 200 Mpa. In figs. 3 to 5 the evolution of the fracture stress is shown together with the inside, mean, and outside hoop stresses in the oxide scale for the three f/m alloys, which we have investigated. According to these results the f/m alloys ST22 and TP91 would be much earlier affected by oxide scale cracking than the f/m alloy HCM12A. For this alloy the outside hoop stress in the oxide scale crosses the fracture stress curve but not the mean hoop stress. This would mean that less than half of the oxide scale should be affected by cracking.

The stress calculations presented and discussed in the foregoing are ,of course, only valid in the linear elastic case, that means before cracking of the scale. With the occurrence of cracking the stresses in the scale are released to a good extent and with further growth of the scale a new stress cycle evolves. We guess that the growth of the scale continues at the outside of the intact part (austenitic alloys) or at its outside and inside (f/m alloys), and that the cracked part of the scale is merely displaced ahead of the intact part. With a new cracking event part of the newly formed intact scale is cracked. The data suggest that cracking

increases linearly with time, that means the lapse of time needed to reach a stress level sufficient for cracking should be roughly constant over the whole exposure time.

An experimental program would be needed for the validation of the model for the growth stresses presented and discussed in this section. In the frame of such a program one should try to determine the onset of cracking in the oxide scale and the evcolution of the fractured part. The creep of the metallic substrate on the other hand leads to creep strains, which could eventually be measured.

## 3.2   Stresses upon temperature changes

These stresses arise due to the differences in the thermal expansion of the oxide scale and the metallic substrate.

Force equilibrium:

$$\sigma_\theta^{ox}\delta^{ox} + \sigma_\theta^{me}s^{me} = 0 \qquad (28)$$

and continuity of hoop strain at the interface oxide/metal:

$$\frac{1-\nu}{E^{ox}}\sigma_\theta^{ox} + \alpha^{ox}\Delta T = \frac{1-\nu}{E^{me}}\sigma_\theta^{me} + \alpha^{me}\Delta T \qquad (29)$$

lead to the following equations for the hoop stresses in the oxide scale and the metallic substrate:

$$\sigma_\theta^{ox} = \frac{E^{ox}}{1-\nu}\frac{(\alpha^{me}-\alpha^{ox})\Delta T}{1+\dfrac{\delta^{ox}}{s^{me}}\dfrac{E^{ox}}{E^{me}}} \qquad (30)$$

$$\sigma_\theta^{me} = -\frac{\delta^{ox}}{s^{me}}\sigma_\theta^{ox} \qquad (31)$$

Due to the isotropic nature of the thermal expansion we have a bi-axial stress state in the cladding with:

$$\sigma_\theta^{me,ox} \cong \sigma_z^{me,ox} \gg \sigma_r^{me,ox} \qquad (32)$$

It is understood that the cladding is in a homogeneous temperature distribution before and after the temperature ramp $\Delta T$. If this is not the case the term $\Delta T\Delta\alpha$ has to be replaced by integrals over the clad wall thickness.

The correction factor $1 + \dfrac{E^{ox}}{E^{me}} \dfrac{\delta^{ox}}{s^{me}}$ arises due to the finite thickness of the metallic substrate. With an infinitely thick substrate this factor would be 1 and we would obtain an expression for the hoop stress in the oxide scale known from the literature.

Calculations have been done for austenitic and ferritic alloys and downward temperature ramps of -100 K, - 300 K, and - 600 K with the material data taken from table 1. The results for the hoop stress are plotted in figs. 9 and 10 as a function of the oxide scale thickness. As the thermal expansion coefficient in the oxide scale is smaller than that in the metallic substrate, we obtain compressive hoop stresses in the oxide scale and tensile stresses in the metallic substrate.

For f/m alloys the difference of thermal expansion coefficients is about 50 % smaller than for austenitic alloys. This is reflected in the hoop stress values. It has been assumed, that we have the same thermal expansion coefficient in the whole oxide scale. But the data found in the literature /3/ suggest that there are differences for the sublayers in the scale of ferritic steels. This would lead to differences in the hoop stresses in the sublayers.

No experimental data for the iron oxides could be found for temperatures above 100°C. Thus, we have taken for $\alpha^{ox}$ the same value as for $Cr_2O_3$. It could well be that the thermal expansion coefficient of iron oxides in the relevant temperature range (300 - 500°C) is a bit higher than $0{,}85 \cdot 10^{-5}$ 1/K. This would then mean that the hoop stress values in case of ferritic martensitic alloys are somewhat lower than that shown in fig. 9.

With compressive stresses in the oxide scale there are two routes for scale cracking and spalling namely a wedging and a buckling mechanism depending on the mechanical properties of the scale and the interface (see for example ref. /2/). The buckling mechanisms is only important for crack-like defects in the interface with a radius much larger than the scale thickness/12/. Thus, the mechanism relevant in our case should be the wedging process, as we do not expect so large defects in the interface.

If W* is the elastic strain energy per unit volume, then the following criteria for the cracking of the scale has been proposed by U.R. Evans /13/.

$$\delta^{ox} W^* \geq \gamma \tag{33}$$

where $\gamma$ is the fracture energy per unit area of the interface. For a bi-axial stress state the elastic energy W* is given as:

$$W^* = \frac{\sigma_\theta^2}{E^{ox}}(1 - \nu) \tag{34}$$

Thus, we obtain the following expression for the critical temperature ramp $\Delta T^c$

$$\Delta T^{c^2} = \frac{\gamma(1 - \nu)}{E^{ox}}(1 + \frac{E^{ox}}{E^{me}} \frac{\delta^{ox}}{s^{me}}) \frac{1}{\delta^{ox}} \frac{1}{(\Delta\alpha)^2} \tag{35}$$

With the data listed in table 1 we would obtain for a scale thickness of 10 μm a critical temperature ramp of about -390 K for ferritic alloys and about -130 K for austenitic alloys.

10

## 3.3 Thermal stresses by radial temperature gradients

As in the foregoing section we have a bi-axial stress state arising due to the difference in thermal expansion, but in this case due to the temperature gradient in each material. Thus we have for the metallic substrate and the oxide scale the following hoop stress increments between inside and outside locations:

$$\Delta \sigma_\theta^{me} = \frac{\alpha^{me} \Delta T^{me} E^{me}}{1-\nu} \tag{36}$$

$$\Delta \sigma_\theta^{ox} = \frac{\alpha^{ox} \Delta T^{ox} E^{ox}}{1-\nu} \tag{37}$$

where $\Delta T^{me,ox}$ are the temperature differences between inside and outside of each layer. To a good approximation we have in both materials linear stress distributions. They can be determined with the help of the continuity condition of the hoop strain at the interface., which leads to the following equation:

$$\sigma_\theta^{me,o} = \frac{E^{me}}{E^{ox}} \sigma_\theta^{ox,i} \tag{38}$$

With the help of the force balance:

$$\overline{\sigma_\theta^{me}} s^{me} + \overline{\sigma_\theta^{ox}} \delta^{ox} = 0 \tag{39}$$

we obtain the following equation for the average hoop stress in the metallic substrate:

$$\overline{\sigma_\theta^{me}} = -\frac{\Delta \sigma_\theta^{me} \dfrac{E^{ox}}{E^{me}} + \Delta \sigma_\theta^{ox}}{2(\dfrac{s^{me}}{\delta^{ox}} + \dfrac{E^{ox}}{E^{me}})} \tag{40}$$

Thus, the inside and outside hoop stresses in the metallic substrate and in the oxide scale are given as:

$$\sigma_\theta^{me,i} = \overline{\sigma_\theta^{me}} - 1/2 \Delta \sigma_\theta^{me} \tag{41}$$

$$\sigma_\theta^{me,o} = \overline{\sigma_\theta^{me}} + 1/2 \Delta \sigma_\theta^{me} \tag{42}$$

$$\sigma_\theta^{ox,i} = \frac{E^{ox}}{E^{me}} \sigma_\theta^{me,o} \tag{43}$$

$$\sigma_\theta^{ox,o} = \sigma_\theta^{ox,i} + \Delta \sigma_\theta^{ox,i} \tag{44}$$

and:

$$\overline{\sigma_\theta^{ox}} = \sigma_\theta^{ox,i} + 1/2\Delta\sigma_\theta^{ox} \tag{45}$$

If there is no oxide scale present, then the expressions simplify to:

$$\sigma_\theta^{me,i} = -1/2\Delta\sigma_\theta^{me} \tag{46}$$

$$\sigma_\theta^{me,o} = 1/2\Delta\sigma_\theta^{me} \tag{47}$$

For simplicity we assume that the heat is predominantly produced in the fuel. If the linear rod power is $\chi$, we have the following temperature gradients in both layers:

$$\Delta T^{me} = \frac{\chi}{2\Pi\lambda^{me}}\ln(r^{me,o}/r^{me,i}) \tag{48}$$

$$\Delta T^{ox} = \frac{\chi}{2\Pi\lambda^{ox}}\ln(r^{ox,o}/r^{ox,i}) \tag{49}$$

With the parameters listed in table 1 we obtain the stress distributions shown in fig. 11. Thus, for a linear rod power of 400 W/cm we would for austenitic alloys obtain an outside hoop stress in the oxide scale of about 185 Mpa, a stress level which could lead to cracking. For ferritic alloys the outside hoop stress would amount to about 145 MPa.

If the metallic substrate can creep, stresses in this material can relax to a certain extent; and the stress level in the oxide scale can be considerably reduced. But the calculation of the creep relaxation process is in this case beyond the scope of the OXSPA code, as we have stress and temperature gradients in the metal phase.
No values for the thermal conductivity of $Cr_2O_3$ could be found in the literature. As a first reasonable guess it was assumed that $\lambda^{ox} = 1/5\ \lambda^{me}$, based on data for $ZrO_2$.


### 3.4   Stresses due to inside and outside pressures

The presence of intact oxide scales increases the strength of the cladding. The main purpose of this section is to investigate the consequences of this effect on fuel rod design. Thus, the respective calculations are for inside and outside pressure values as obtained from design calculations for the target burn-up.

Two different solutions are implemented in the OXSPA code. The first solution is based on a finite difference approximation of the stress equilibrium condition in the tube and the second solution is based on the Lame equations. We start with the first solution.

The following equilibrium condition is valid for cylindrical tubes:

$$r\frac{d\sigma_r}{dr} = \sigma_\theta - \sigma_r \tag{50}$$

The finite difference approximation to this equation, applied for a certain layer in the cladding reads as follows:

12

$$\bar{r}\frac{\sigma_r^o - \sigma_r^i}{r^o - r^i} = \overline{\sigma_\theta} - \overline{\sigma_r} \tag{51}$$

with :

$$\bar{r} = 1/2(r^i + r^o) \tag{52}$$

$$\overline{\sigma_{r,\theta}} = 1/2(\sigma_{r,\theta}^i + \sigma_{r,\theta}^o) \tag{53}$$

With the boundary conditions:

$$\sigma_r^{i,o} = -p^{i,o} \tag{54}$$

we obtain:

$$\overline{\sigma_\theta} = (p^i - p^o)\frac{\bar{r}}{s} - 1/2(p^i + p^o) \tag{55}$$

with s = $r^o$ - $r^i$ and $p^i$ and $p^o$ being the inside and outside "pressures".

The equation (55) can be applied to the metallic substrate and the oxide scale:

$$\overline{\sigma_\theta^{me}} = (p^i - p^{int})\frac{\overline{r^{me}}}{s^{me}} + \overline{\sigma_r^{me}} \tag{56}$$

$$\overline{\sigma_\theta^{ox}} = (p^{int} - p^o)\frac{\overline{r^{ox}}}{\delta^{ox}} + \overline{\sigma_r^{ox}} \tag{57}$$

The unknown "pressure" at the interface $p^{int}$ can be determined with the help of the continuity condition for the hoop strain, which leads to:

$$\overline{\sigma_\theta^{ox}} = \frac{E^{ox}}{E^{me}}\overline{\sigma_\theta^{me}} \tag{58}$$

so that we finally obtain:

$$p^{int} = (p^o(\frac{\overline{r^{ox}}}{\delta^{ox}} + 1) + p^i\frac{E^{ox}}{E^{me}}(\frac{\overline{r^{me}}}{s^{me}} - 1)) / (\frac{\overline{r^{ox}}}{\delta^{ox}} + \frac{E^{ox}}{E^{me}}\frac{\overline{r^{me}}}{s^{me}}) \tag{59}$$

The thickness of the metallic substrate can be calculated according to:

$$s^{me} = s^0 - \frac{\delta^{ox}}{\varphi} \tag{60}$$

$s^0$ = the as-fabricated clad wall thickness

Results of calculations for the ferritic alloy HCM12A are shown in figs. 12 to 13 with and without taking into account the strengthening effect of the oxide scale in the stress calculations. The values of the parabolic oxide scale thickness at a temperature of 650 $^0$C

and the inner pin pressure at different times of operation are listed in table 4,as they were obtained from the oxidation correlation for this alloy and from design calculations of the fission gas pressure /14/. The oxidation correlation of the austenitic alloy 1.4910 gives roughly the same values for the oxide scale thickness, for example at an operational time of 45000 h we obtain a value of 133 μm for this austenitic alloy. This is only slightly lower than the respective value of 136 μm for the ferritic alloy HCM12A. Therefore the stress results obtained for the ferritic alloy HCM12A are to a good approximation also valid for the austenitic alloy 1.4910. If one takes the strengthening effect of the oxide scale into account, Young's modulii of the metal and of the oxide play a role and this makes that both alloys have slightly different stress values.

Under normal operational conditions the coolant pressure is 25 Mpa but in case of an accident we have to take a value of 0 Mpa for the outer pressure. Stress calculations have been done in each case for both values of outer rod pressure. Therefore we have in each figure four stress curves. For design considerations the hoop stress in the metallic substrate is decisive. Therefore we have concentrated on this aspect. Under normal operation we obtain compressive hoop stresses and under safety conditions tensile stresses in the cladding. If one takes the strengthening effect of the oxide scale into account the loading of the metallic substrate is reduced.

An important parameter constitutes also the as-fabricated clad wall thickness. A range of 0.4 to 0.7 mm has been taken in the calculations for this parameter. The higher the as-fabricated clad wall thickness the lower is the mechanical loading of the cladding. The increase of the in pin gas pressure is under normal operation beneficial for the mechanical loading of the cladding, as the difference between inner and outer pressure decreases. If the mechanical effect of the oxide scale is neglected, the decrease of the metallic layer thickness counterbalances the pressure effect to some extent up to an operational time of about 10000 h. Afterwards the beneficial effect of the in pin gas pressure increase dominates in any case.

**Table 4:**   Values of the oxide scale thickness at 650 $^{0}$C of the ferritic alloy HCM12A and of the in pin gas pressure at different operational times

| time (h) | $\delta^{ox}$(um) | $p^{in}$(Mpa) |
|---|---|---|
| 0 | 0 | 8.0 |
| 10000 | 64 | 10.2 |
| 20000 | 91 | 12.4 |
| 30000 | 111 | 14.6 |
| 40000 | 128 | 16.8 |
| 45000 | 136 | 17.9 |

When the pressure in the coolant channel is higher than the inside gas pressure, we obtain compressive hoop stresses in the oxide scale and in this case there may be no doubt about the strengthening effect of the oxide scale. In the LOCA case ($p^o$ = 0 Mpa) we obtain tensile hoop stresses in the oxide scale and depending on the values of the fracture stress there can be cracking of the scale and the strengthening effect will be lost.

The foregoing approximate solution of the stress problem was based on a finite difference expression of the equilibrium condition for the stresses in the cylindrical tube, and mean values can successfully be applied only for thin-walled tubes. For thick-walled tubes one must take recourse to the Lame stress equations /15/. These are in the elastic case the exact solutions of the stress problem in a cylindrical tube with inside and outside pressures. The Lame solution can ,of course, be used to check the validity of the approximate solution.

14

The stress functions have the following general form in the metallic substrate and in the oxide scale:

$$\sigma_r^{me}(r) = A^{me} + \frac{B^{me}}{r^2} \tag{61}$$

$$\sigma_\theta^{me}(r) = A^{me} - \frac{B^{me}}{r^2} \tag{62}$$

$$\sigma_r^{ox}(r) = A^{ox} + \frac{B^{ox}}{r^2} \tag{63}$$

$$\sigma_\theta^{ox}(r) = A^{ox} - \frac{B^{ox}}{r^2} \tag{64}$$

Thus, these solutions depend on 4 free parameters, which have to be determined with the help of 4 boundary conditions:

$$\sigma_r^{me}(r^i) = -p^i \tag{65}$$

$$\sigma_r^{ox}(r^o) = -p^o \tag{66}$$

$$\sigma_r^{ox}(r^{int}) = \sigma_r^{me}(r^{int}) \tag{67}$$

$$\varepsilon_\theta^{ox}(r^{int}) = \varepsilon_\theta^{me}(r^{int}) \tag{68}$$

The solution of these equations is a lengthy task and shall not be repeated here. But we can note that the 4 parameters $A^{me/ox}$ and $B^{me/ox}$ depend on the 3 radii $r^i$, $r^o$, and $r^{int}$ , the inside and outside pressures $p^i$ and $p^o$ and the Young's moduli $E^{ox}$ and $E^{me}$ and the Poisson number $\upsilon$.

The results of a calculation for the ferritic alloy HCM12A are to be found in fig. 14. In this figure are also noted the parameters which have been used for the calculation, namely an as-fabricated clad wall thickness of 0.4 mm, for example. The stresses depend in this case on the radial position with a nearly linear dependence. The mean value of the hoop stress in the metallic substrate is about 112 MPa, whereas with the approximate solution we obtained a value of about 115 MPa.

## 4    Conclusion

Simple analytical models for solutions of different stress problems in cylindrical tubes of austenitic and ferritic/martensitic alloys with oxide scales have been developed and implemented in the code OXSPA. They allow to gain direct insight into the situation and to discern the main physical parameters, which determine the behavior of the compound oxide scale/ metallic substrate and are therefore most valuable for design considerations.

## 5    References

[1]    M. Schütze:
Mechanical Properties of Oxide Scales, Ox. Of Met., Vol. 44, pp 29-61, 1995

[2]    H.E. Evans:
Modeling oxide spallation, Mat. High Temp., Vol. 12, pp 219-237, 1994

[3]    Gmelins Handbuch der Anorganischen Chemie, Verlag Chemie, Weinheim, 1970

[4]    C. Petersen:
Literaturübersicht mechanischer und physikalischer Eigenschaften von Hüllwerkstof-
fen für Fortgeschrittene Druckwasserreaktoren (FDWR) bei hoher Temperatur, KfK
3469, 1983

[5]    L. Heikinheimo: private communication

[6]    M. Schirra: private communication

[7]    M. I. Manning:
Geometrical Effects on Scale Integrity, Corr. Science, Vol. 21, pp. 301-316, 1981

[8]    S. Espevik, et al:
Oxidation of Ni-Cr-W Ternary alloys, Oxidation of Metals, Vol. 14 pp. 85-109,
1980

[9]    G. Müller:
Korrosionsverhalten von Stählen in flüssigem Blei nach Behandlung mit hochenerge-
tischen gepulsten Elektronstrahlen, FZKA 6422, 2000

[10]    G. C. Stoney,
Proc. R. Soc., London A82, p.172, 1909

[11]    M.I. Manning and D.B. Meadowcroft, unpublished

[12]    H. Steiner, M. Heck:
Stresses in an Oxidized Zircaloy Cladding under Quench Conditions, Nucl. Techn.
Vol. 123, pp. 209-221, 1998

[13]    U.R. Evans:
An Introduction to Metallic Corrosion, Edward Arnold, London, 1948

[14]    K. Ehrlich, private communication

[15]    J. Chakrabarty:
Theory of Plasticity, Mcgraw-Hill Intern. Edit. ,N.Y., p.316, 1987

## Notation

| | | |
|---|---|---|
| $\sigma$ | = | stress |
| $\epsilon$ | = | strain |
| $T$ | = | temperature |
| $t$ | = | time |
| $E$ | = | Young's modulus |
| $\nu$ | = | Poisson-number |
| $\varphi$ | = | Pilling/Bedworth-ratio |
| $\alpha$ | = | thermal expansion coeff. |
| $K_I$ | = | fracture toughness |
| $\gamma$ | = | fracture energy |
| $r$ | = | radius |
| $\delta$ | = | scale thickness |
| $s$ | = | wall thickness |
| $a$ | = | original clad outer radius |
| $c$ | = | flaw size |
| $w$ | = | strain energy |

## Indices

| | | |
|---|---|---|
| $ox$ | = | oxide |
| $me$ | = | metallic |
| $i$ | = | inner |
| $o$ | = | outer |
| $\theta$ | = | azimuthal |
| $z$ | = | axial |
| $r$ | = | radial |
| $eq$ | = | equivalent |
| $f$ | = | fracture |
| $c$ | = | critical |
| $sw$ | = | swelling |
| $V$ | = | volume |
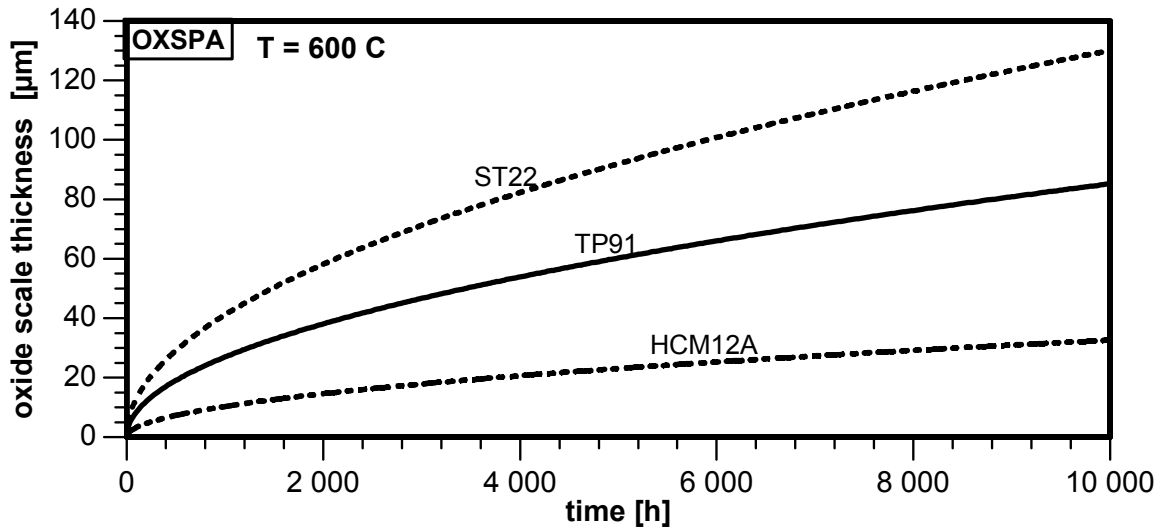
Fig. 2: Evolution of the parabolic contribution to the oxide scale thickness for three f/m alloys
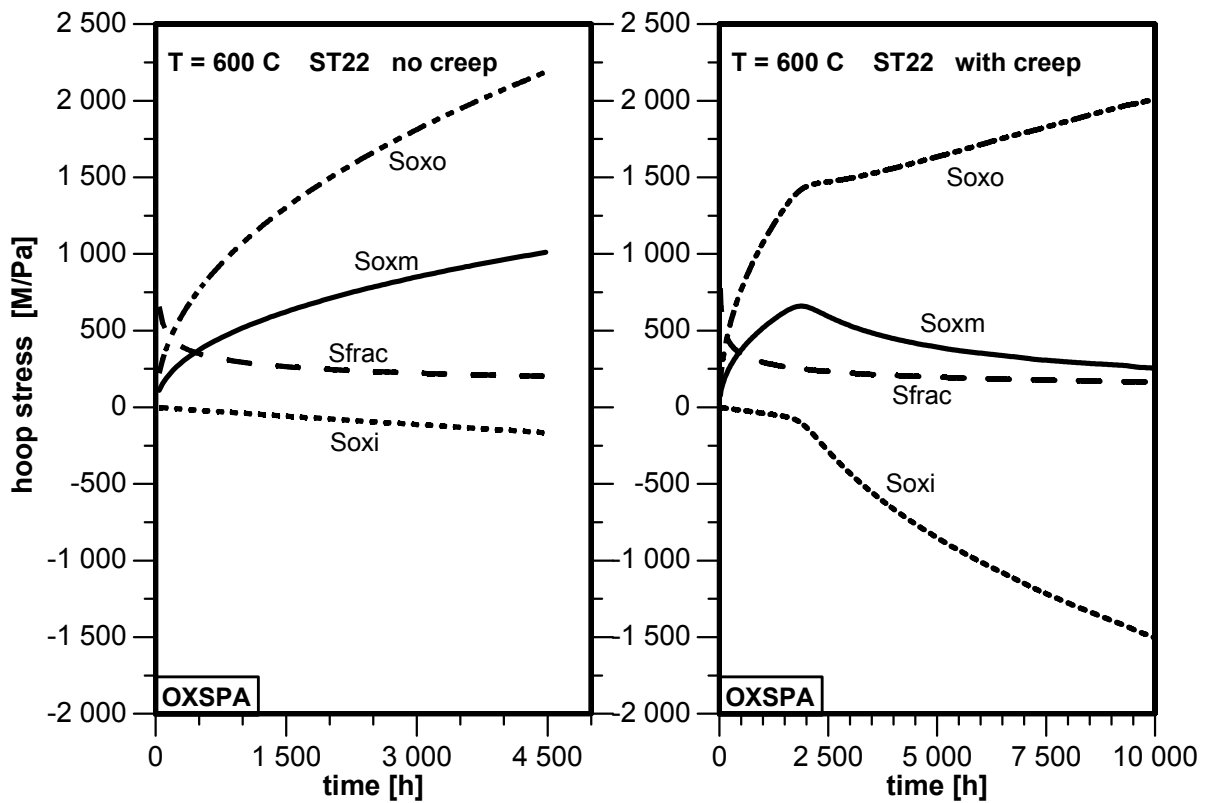


Fig. 3:    Evolution of the hoop stresses in the oxide scale of the f/m alloy ST22 with and without creep in the metallic substrate and the fracture stress acc. to ref. [11]
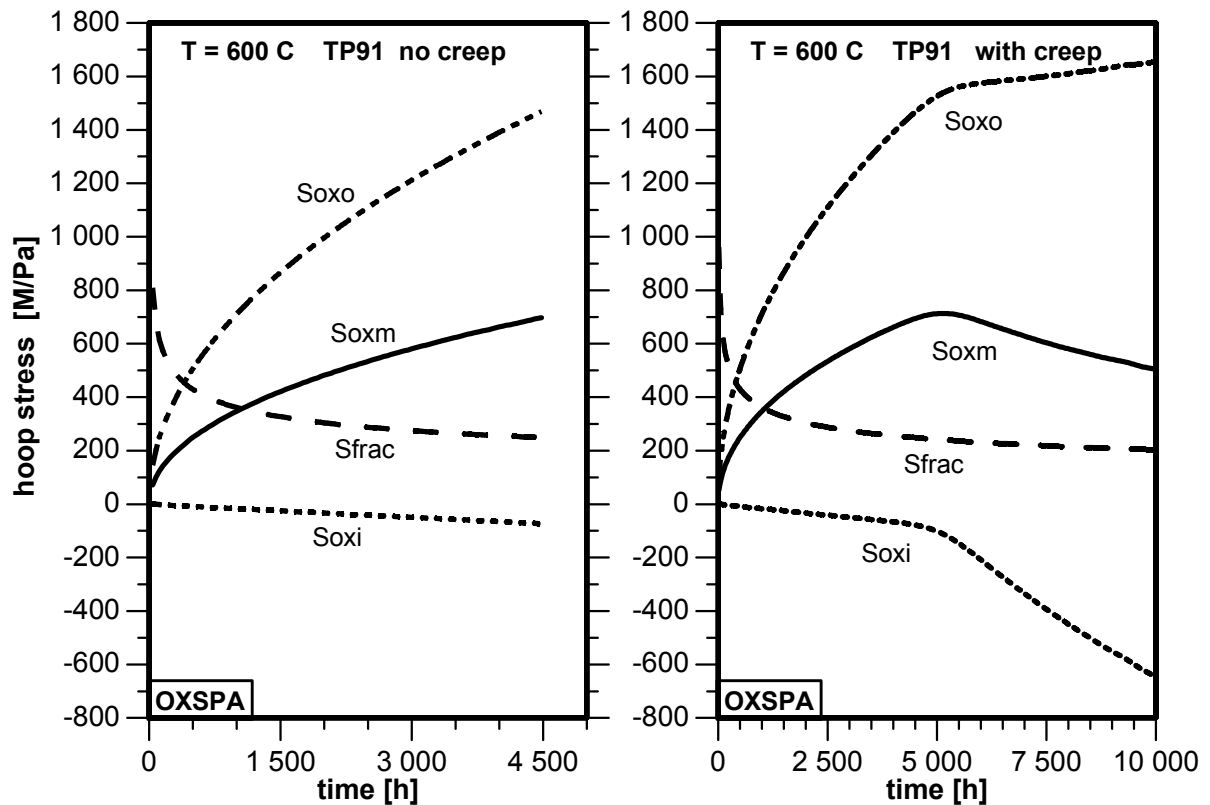
Fig. 4: Evolution of the hoop stresses in the oxide scale of the f/m alloy TP91 with and without creep in the metallic substrate and the fracture stress acc. to ref. [11]
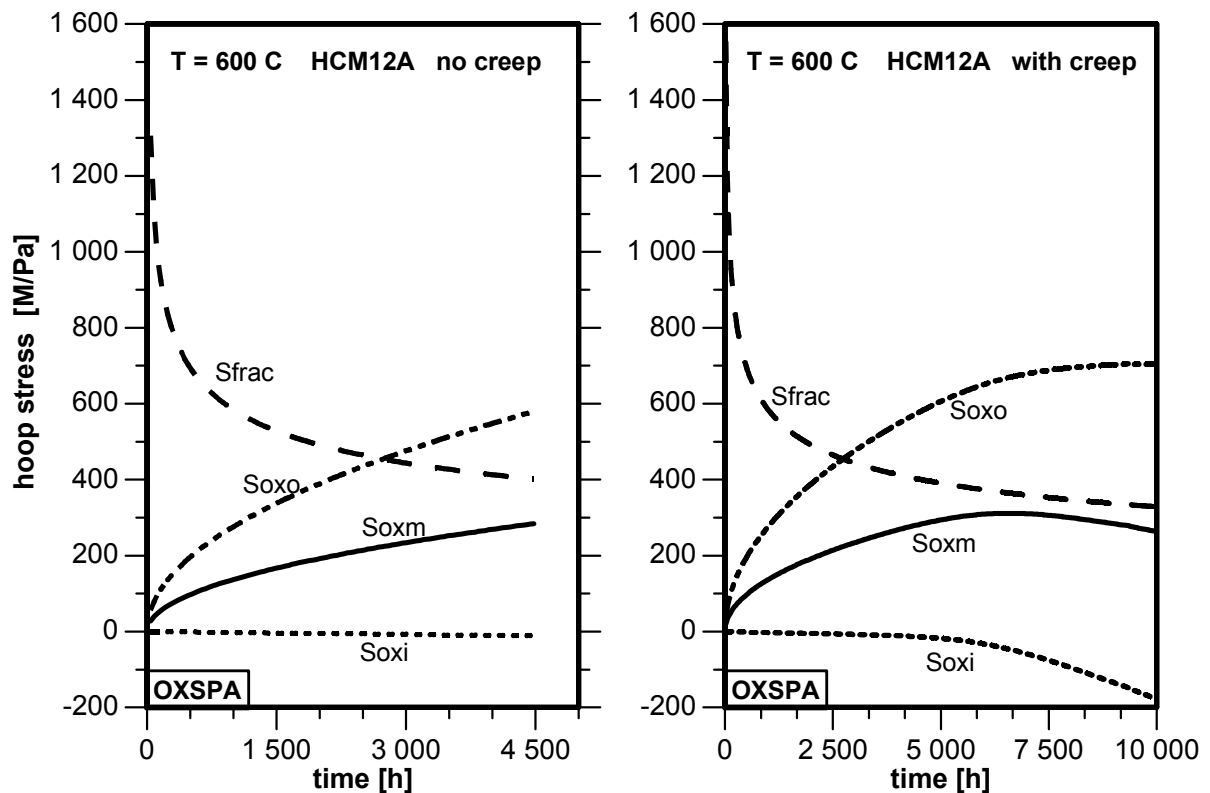


Fig. 5: Evolution of the hoop stresses in the oxide scale of the f/m alloy HCM12A with and without creep in the metallic substrate and the fracture stress acc. to ref. [11]
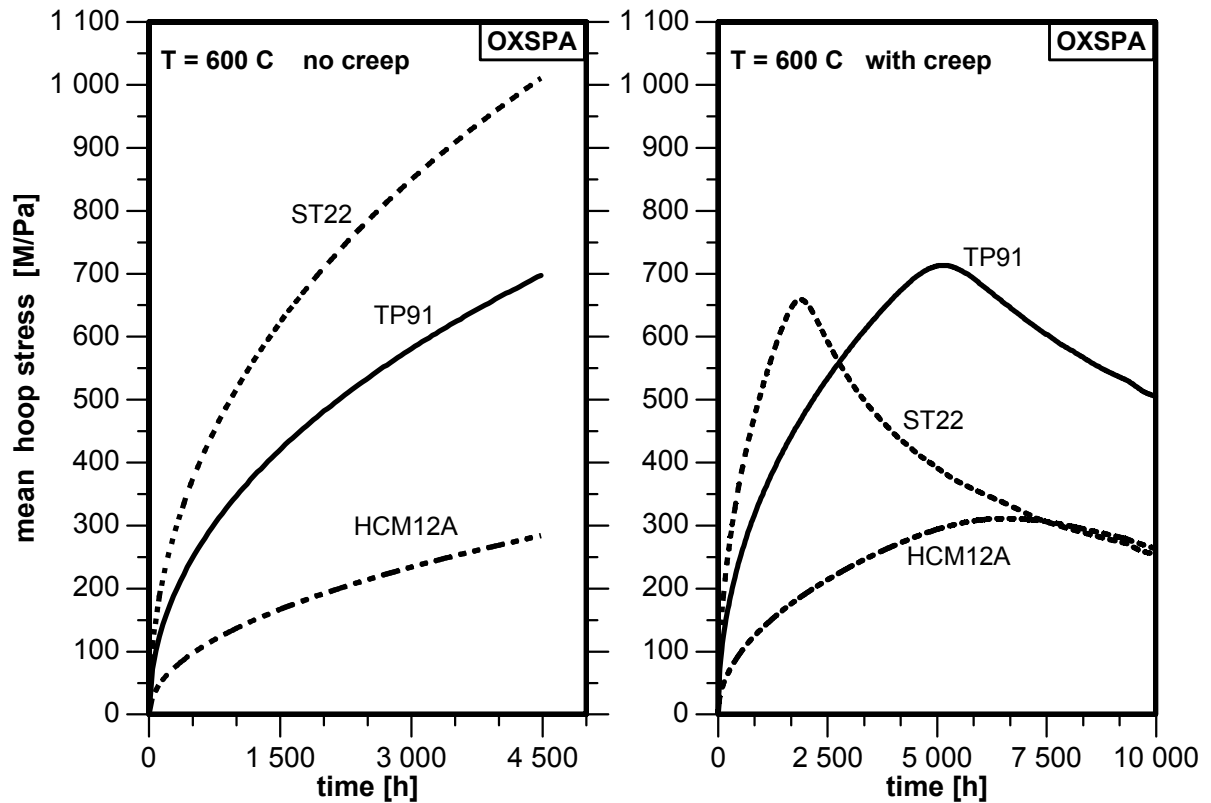
Fig.6:    Evolution of the mean hoop stress in the oxide scale for three f/m alloys with and without creep in the metallic substrate
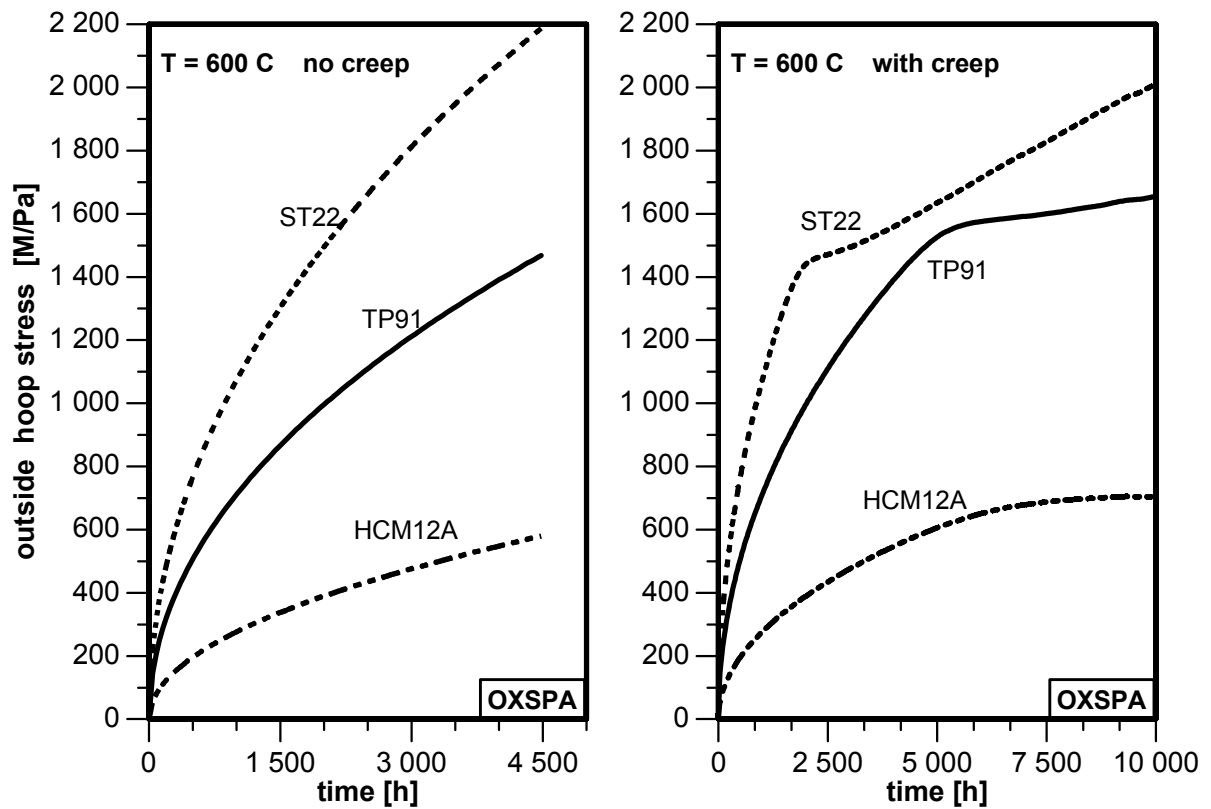


Fig. 7:    Evolution of outside hoop stress in the oxide scale for three f/m alloys with and without creep in the metallic substrate taken into account

20
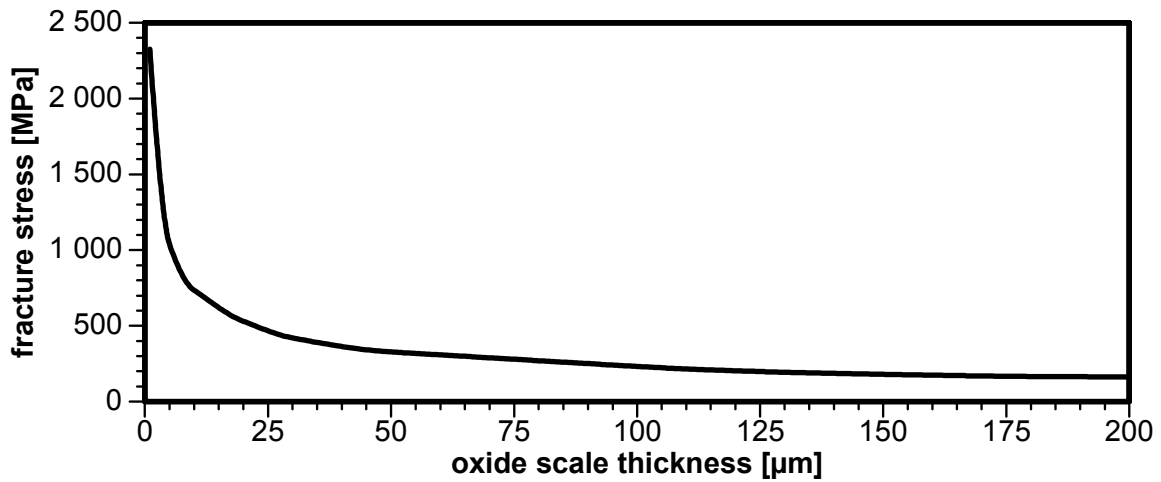
Fig. 8:     Fracture stress in the oxide scale versus the oxide scale thickness acc. to ref. [11]
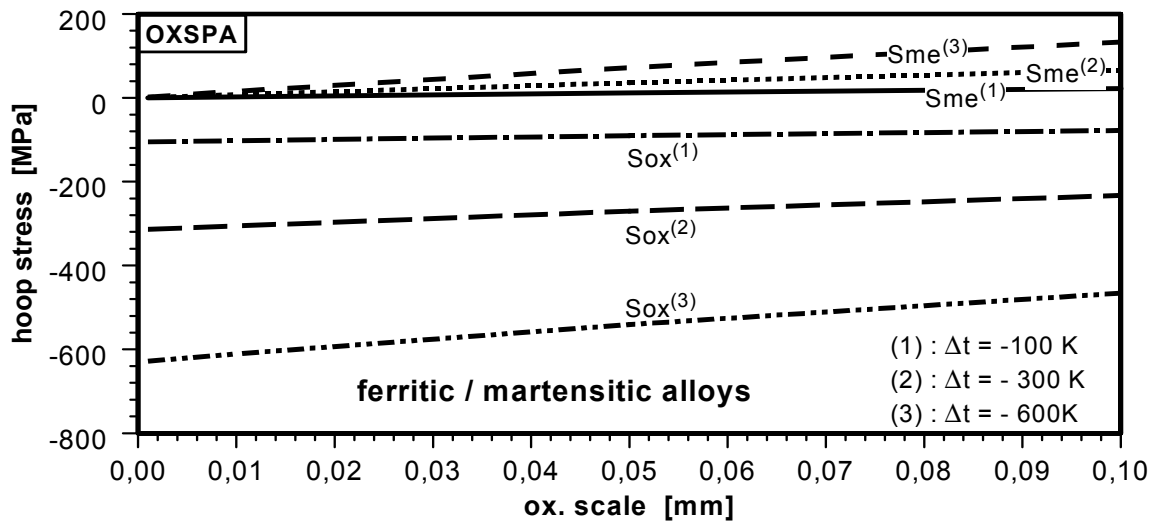


Fig. 9:     Hoop stress in the ox. scale and the met. substrate for different temp. ramps
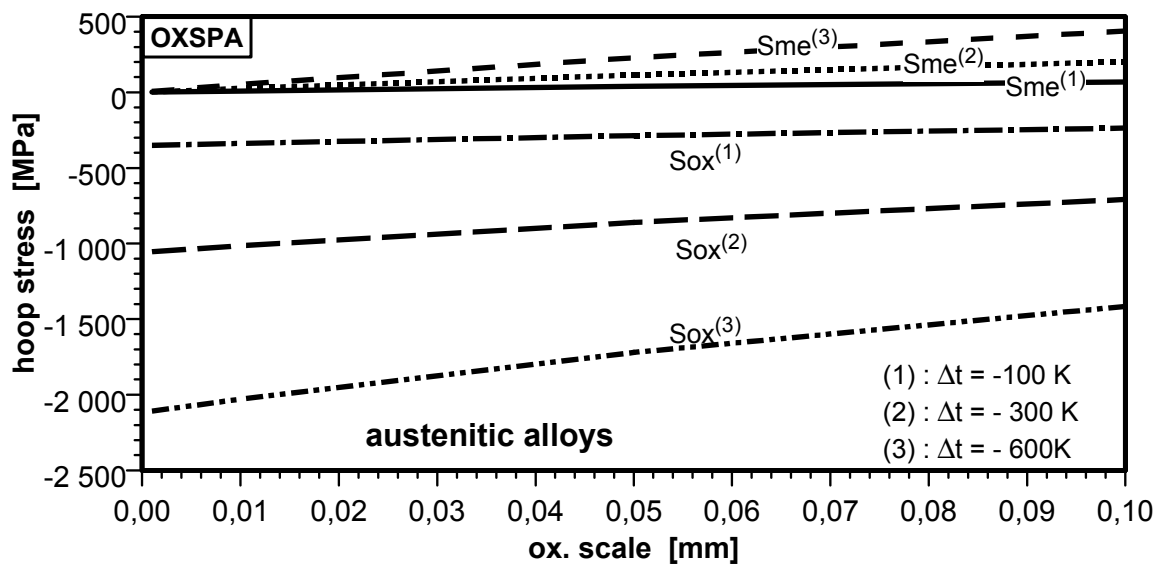


Fig. 10:    Hoop stress in the ox. scale and the met. substrate for different temp. Ramps
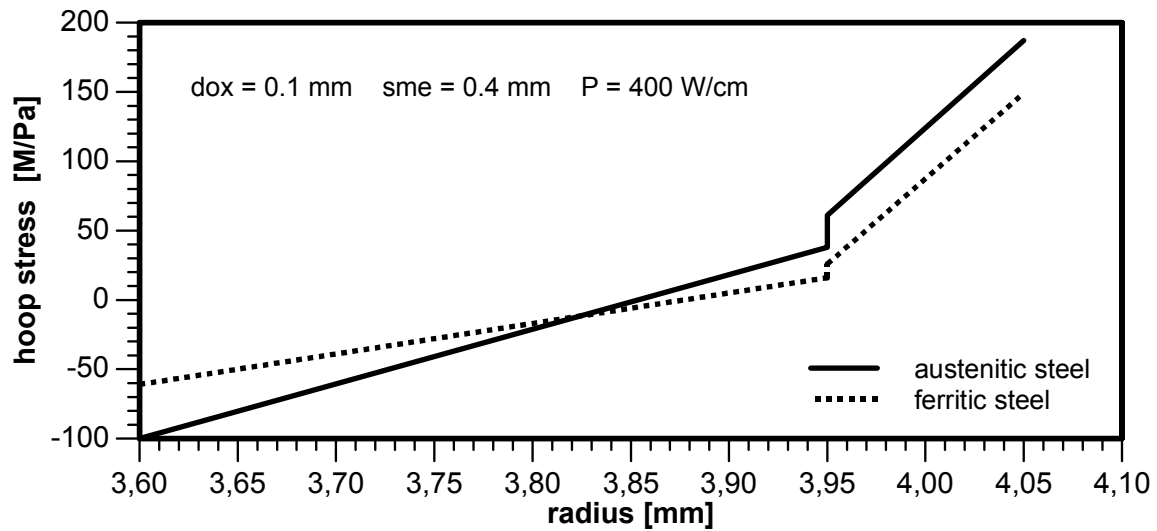
Fig. 11    Radial hoop stress distribution in an oxidized cladding due to a radial temp. gradient
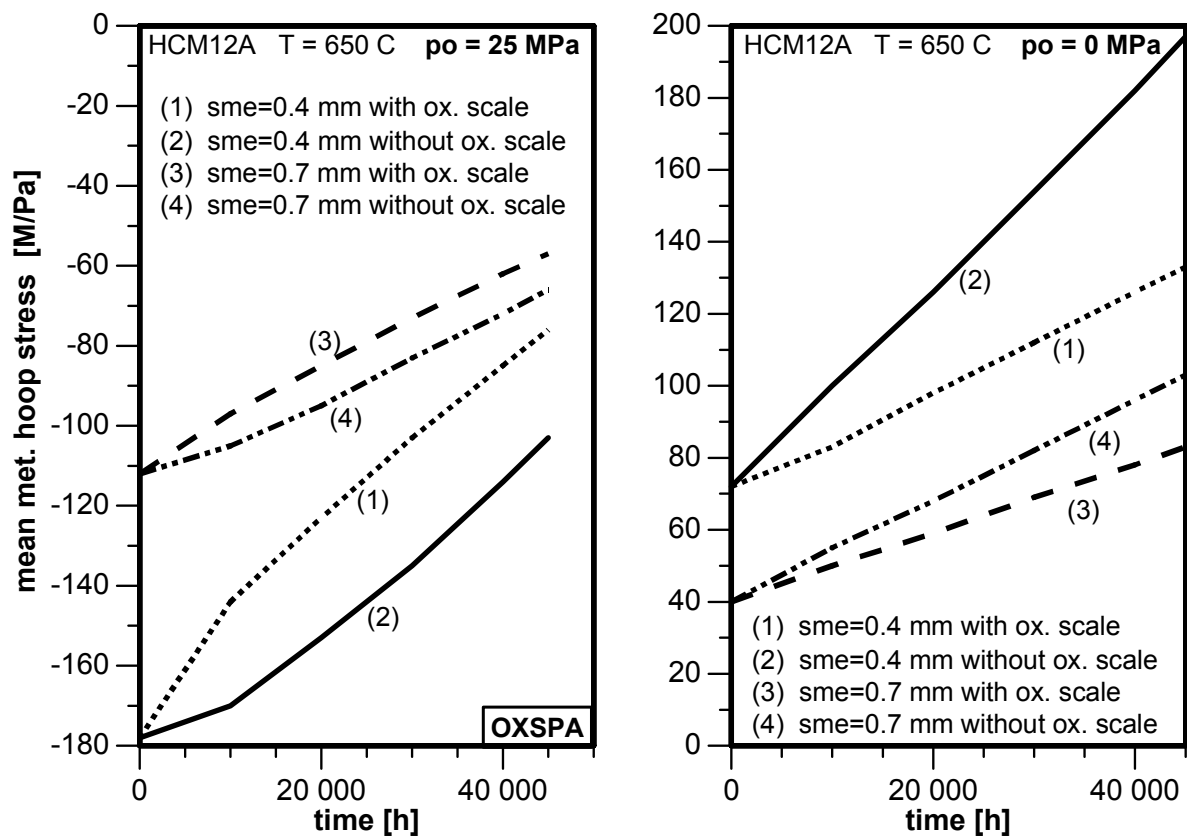


Fig. 12+13: Evolution of the mean hoop stress in the met. substrate for two values of the as-fab. clad wall thickness with and without taking into account the strengthening effect of the oxide scale
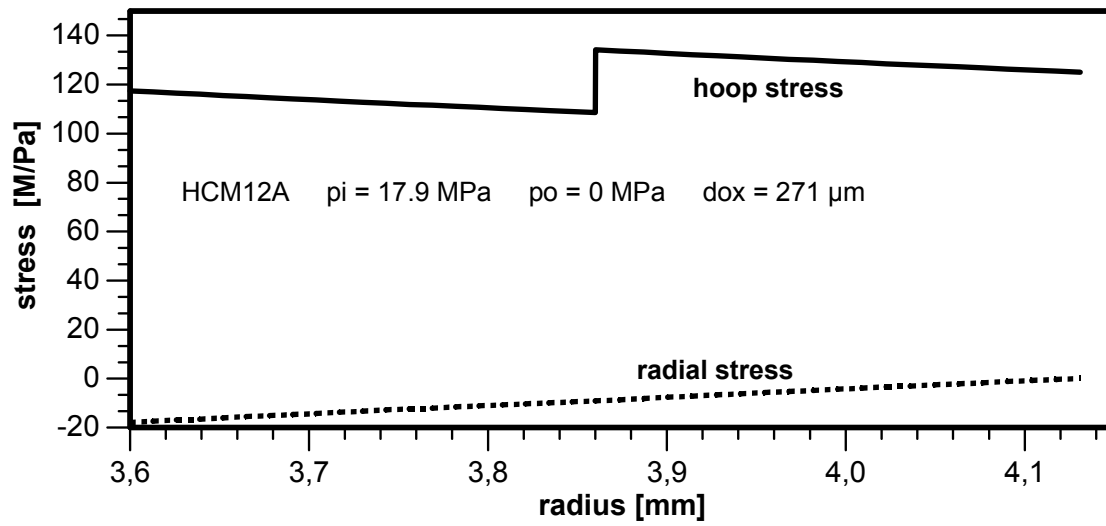
Fig. 14: Radial distribution of stresses in an oxidized cladding acc. to the lame solutions